Applied Ocean Research 25 (2003) 167–186

Applied Ocean Research

www.elsevier.com/locate/apor

On estimating extreme wave heights using combined Geosat, Topex/Poseidon and ERS-1 altimeter data

Jose Henrique G.M. Alves[a], Ian R. Young[b,*]

[a]Marine Modeling and Analysis Branch, Environmental Modeling Center, NCEP/NOAA, USA
[b]Swinburne University of Technology, P.O. Box 218, Hawthorn, Vic. 3122, Australia

Received 31 March 2003; accepted 21 January 2004

Abstract

The estimation of extreme significant wave heights H_s using altimeter observations is investigated. Data from the following three satellite missions are used: Geosat, ERS-1 and Topex/Poseidon. Practical methods of estimating extreme H_s are described and limitations of their application to altimeter data are highlighted. Extreme H_s are estimated using the three-parameter Weibull distribution, with maxima selected via the peaks over threshold method, and the Fisher-Tippet type I distribution, using data selected via the initial distribution method. Altimeter estimates are compared to extreme H_s calculated from deep water buoy data. A comparative analysis of global estimates of satellite-derived extreme H_s based on standard statistics investigates time-space undersampling and how it affects the reliability of long-term extreme wave estimates made using satellite altimeter data.

1. Introduction

Extreme values of significant wave height H_s with long term return periods are fundamental parameters in several ocean engineering and oceanographic applications. These include coastal management, naval architecture, navigation and several issues related to coastal and offshore structures. As a consequence of the large concentration of human settlements along the coastline and of economic activities there and across the oceans, extreme events generated within the oceanic environment are among the most hazardous. Consequently, the development of tools to assist in their prediction is an important scientific challenge with a wide range of applications.

The determination of extreme H_s in the oceanic environment usually involves the statistical analysis of historical time series of wave heights derived from surface buoy measurements. The usual practice consists of a number of steps starting with the choice of a statistical model fitting observations of storm H_s or other parameters representative of H_s maxima. The statistical model best fitting the data is then extrapolated beyond the period covered by the observations at a chosen probability level, which is associated with the occurrence of an extreme event with a return period of N years (typically, $N = 50$ or 100).

Except for areas in the northern Atlantic and Pacific oceans, buoy networks generally do not provide adequate resolution or historical coverage of wave data for the purpose of estimating extreme H_s. Either time series are not long enough or the number of existing buoys is too small or both. Engineering applications usually require knowledge of extreme H_s with 50 and 100 year return periods. The reliability of these estimates is thus significantly reduced due to the short time length of the available buoy measurements.

The relatively short period covered by buoy measurements also allows large freedom in selecting the distribution functions that fit the observed data properly, often resulting in several estimated values at a single location that differ significantly. If the short length of the data series obstructs the efforts of estimating extremes in some locations, in others it is not possible at all to make estimates due to the poor spatial coverage and the unavailability of in situ measurements on a global basis. These limitations affect mostly the determination of extreme H_s in oceanic areas adjacent to developing countries in the Southern Hemisphere.

* Corresponding author.
E-mail address: iyoung@swin.edu.au (I.R. Young).

0141-1187/$ - see front matter © 2004 Elsevier Ltd. All rights reserved.
doi:10.1016/j.apor.2004.01.002

Recent advances in atmospheric and wind-wave modeling technology have made it possible to build long-term databases of hindcast wind speeds and wave heights with global coverage [18,23]. The alternative of using these long-term hindcast sea states to calculate global extreme H_s is very attractive, as demonstrated recently by Wang and Swail [31,32]. However, atmospheric and wind-wave models still lack the skill to make accurate predictions or reconstitutions of extreme events, as shown by Cardone et al. and Swail and Cox [2,24].

An attractive alternative to obtaining global estimates of extreme H_s is to use satellite measurements of the sea surface. Since the Seasat experiment in 1978, satellite missions have proved the feasibility of using satellite-borne radar altimeters to obtain reliable wind and wave climatology with global coverage. Although the time span of remotely sensed measurements is still not long enough to overcome problems related to statistical confidence and consistency of statistical extrapolations needed for estimating extreme values, the lack of spatial coverage associated with buoy data is not a major problem when using satellite data. As a consequence, recent studies using altimeter data have developed a preliminary framework for determining extreme H_s on a global basis [3,9,21].

In this study we investigate the adequacy of obtaining global estimates of extreme H_s made with satellite altimeter data, using two methods commonly used to estimate buoy-derived extreme sea states. We calculate long-term extreme H_s using a global satellite altimeter database, consisting of measurements made during the missions of Geosat, ERS-1 and TOPEX/Poseidon, covering a 10-year period. We highlight some difficulties that arise from the sampling characteristics of altimeter data and investigate simple alternatives to reduce this limitation. In this way, we provide a potentially useful approach to obtain information for engineering and oceanographic applications in locations where buoy data are presently unavailable.

This manuscript is structured as follows. In Section 2 we provide a brief description of the combined altimeter database. Commonly used methods for estimating extreme values of environmental variables are outlined in Section 3. Our validation strategy based on comparisons between extreme H_s calculated with satellite data and ocean surface buoy measurements is summarized in Section 4. Results are presented in Section 5, which is followed by a discussion of how these results relate to previous studies in Section 6. Finally, our main conclusions are summarized in Section 7.

2. Combined altimeter database

The combined satellite altimeter database used in our study covers a 10-year period (1986–1995), including Geosat's Exact Repeat Mission (November 1986 to January 1990) and parts of the ERS-1 (August 1991 to August 1995) and the TOPEX/Poseidon (September 1992 to October 1995) missions, totaling 78 months (6.5 years) of effective observations. Young and Holland [29,30] provide details of the methodology used to inter-calibrate, quality-control and merge these data into a single database composed initially of mesh elements covering $2° \times 2°$ in latitude and longitude.

The initial size of mesh elements at $2° \times 2°$ was a compromise between spatial resolution and statistical reliability, based on investigations of the consequences of using different mesh sizes to the consistency of associated wave climate parameters. These investigations [9,26] have indicated that the choice of $2° \times 2°$ mesh elements is close to optimal for wave climatology studies. This data structure has been successfully used by several authors to investigate wave climate using satellite altimeter data [1,3,4,30]. In our study, we investigate the effects on estimates of extreme H_s and the statistical reliability for both $2° \times 2°$ and larger $4° \times 4°$ mesh elements.

The choice of a regular mesh resolution in all locations over the globe, as made in the present study, seems to reflect the current practice and is convenient for generating a global climatology of extremes. However, the adequacy of such an approach and the chosen mesh-element size may not be appropriate for some local applications, particularly in areas where the spatial variability of the wave climate is high due to the proximity of land or other environmental factors. In these cases, local measurements would provide a more reliable source of data for estimating extremes. Studies for determining the local correlation length scales of wave fields, such as that reported in Ref. [16], may lead in the future to a more appropriate selection of location-dependent mesh-element sizes for estimating global extremes considering local wave climatology.

3. Methods for estimating extreme H_s

The N-year extreme value of an environmental variable is a threshold quantity that is exceded on average every N years. In coastal and ocean engineering applications N is usually equal to 50 or 100 years. Our interest is, therefore, on estimating extreme H_s with an average recurrence of 50 or 100 years from a much shorter, 10-year-long database. Thus, the estimates of extreme H_s depend heavily on an approach based on statistical analysis and extrapolation.

Within this framework, the usual procedure for estimating extreme values through statistical extrapolation consists of the following steps:

1. extract from the database of H_s a series representing observed maxima;
2. rank the series of maxima;
3. assign cumulative distribution functions (CDFs) to individual maxima;
4. fit statistical distributions or models to the series of maxima and their CDFs;

5. apply tests to assess goodness of fit;
6. compute the extreme H_s values with a prescribed return period.

Other than the availability of good quality data with a suitable historic coverage, two other factors are critical to obtaining reliable estimates of extreme H_s. One is obviously the choice of statistical distribution used to extrapolate the data to the chosen probability level. The other important factor is the selection of a sub-set of the original database that is representative of the observed maxima.

The selection of a representative series of maxima is very important because it allows the fitting of the chosen statistical model to actual observed maxima. This will generally bring more confidence that the extrapolation to a chosen probability level will be a reliable estimate of a longer-term extreme H_s. On the other hand, fitting a statistical model to all measurements of H_s, for example, may lead to unreliable estimates of longer-term extremes, since the probability distribution of H_s maxima does not necessarily follow a distribution that fits well all observations of H_s. Further discussion on this topic is found in Refs. [17,20,25], for example.

In this context, the three most commonly used techniques to produce sub-sets of data for investigating extreme waves are the initial distribution method (IDM), the annual maxima method (AM) and the peaks over threshold method (POT). A brief description of their main characteristics is provided below.

(a) IDM

In the IDM all available measurements, whether associated or not with storm events, are binned into ascending classes of wave heights. This means that IDM data using one- to three-hourly measurements, common for buoy data, are likely to include multiple values generated by the same storm. Consequently, the estimates of extreme H_s will be made using a statistical model adjusted to a distribution of H_s that does not necessarily describe properly the distribution of maxima. Although in principle this can lead to biased and/or unreliable estimates of extreme H_s, studies using both buoy and satellite observations from the North Sea [6] have shown that the IDM can be used to provide acceptable estimates of environmental extremes.

(b) AM

In the AM method only the highest H_s observed in any particular year is chosen, thus providing a series of uncorrelated observations. A shortcoming of the application of this method to estimating extreme wave heights is that the period covered by measurements of H_s is generally limited to a relatively small number of years, which not surprisingly leads to series of annual maxima that are too short to yield reliable results. In addition, when satellite data are considered, the existence of large time lags between consecutive satellite passes over any given location, results in undersampling of sea-state maxima, leading to an underestimation of AM values relative to buoy data. An example of the effects of this limitation and a discussion of its consequences for obtaining representative series of storm H_s using POT data are presented in Section 5.

(c) POT

The POT method has been nominated by a working group on extreme waves associated with the International Association for Hydraulic Research (IAHR) as the recommended choice for estimating extreme H_s [15,19,28]. This method consists of extracting from a database containing measurements of H_s, values that exceed a given threshold. Such values should also be separated by time lags large enough to guarantee the selection of independent observations, i.e. maximum H_s observed during different storm events.

The choice of thresholds for censoring data in the POT method can be somewhat subjective. For the purposes of automation of the analysis, a common but rather arbitrary approach is to adjust the threshold to increase or decrease the number of extracted maxima until the best fit between observations and a chosen statistical model is achieved. A more objective method that is also consistent with the physics of the generation of extremes consists of first estimating the number of expected local maxima for a given location. The threshold H_s is then selected so that the resulting number of observed maxima does not exceed the number of storms per year at the site. This number may be determined in many different ways (e.g. through the analysis of weather charts or storm databases).

The IAHR recommended practice may be summarized by the following steps:

1. select from a database a subset of H_s maxima using the POT method;
2. separate the subset of H_s maxima into new subsets with data from different storm populations;
3. fit the three-parameter Weibull distribution to the POT data from each subset;
4. compute the desired extreme H_s values associated with each storm population.

Modifications of this methodology are required when using a large global database composed of satellite observations. The analysis of individual storm events necessary to satisfy the POT criterion would be prohibitive on this global scale. In our case, a practical approach is to use a storm database [10] giving the average annual numbers of storms at the center of each $2° \times 2°$ ($4° \times 4°$) mesh element. If an automated procedure is to be used, separating storms from different populations is also not viable. Thus, at any given $2° \times 2°$ mesh element all data are taken as belonging to the same storm population, which may limit the reliability of estimated extreme H_s in areas exposed to more than one type of storm (e.g. tropical and extratropical storms).

4. Validation strategy

An investigation of the compatibility between wave measurements made by satellite altimeters and ocean-surface buoys was made by Cooper and Forristall [9], through the analysis of simulated storm winds and waves generated with simple parametric models. They conclude that satellite measurements made within a radius between 100 and 300 km centered at a given point generally provide equivalent information to hourly buoy measurements made at the central point. Thus, the results of Cooper and Forristall [9] suggest that, in principle, single-point buoy data and satellite measurements made within areas roughly the size of $2° \times 2°$ and up to $4° \times 4°$ mesh elements should all provide similar estimates of extreme H_s. Consequently, it would be reasonable to expect that a global database of satellite altimeter measurements of H_s, such as the one used in this study, would potentially address the objectives of obtaining reliable global estimates of long-term extreme H_s, given a proper choice of statistical model is made for the purposes of extrapolation.

To verify if these assumptions, based on the findings of Cooper and Forristall [9], are valid to our combined satellite database, we compare extreme H_s calculated from altimeter data and deep water in situ wave measurements made with ocean surface buoys. A total of 11 buoys deployed in the northern Pacific and Atlantic oceans are used. Data from 10 buoys were obtained from the National Data Buoy Center (NDBC) of the US National Oceanic and Atmospheric Administration (NOAA). Data from the eleventh buoy location, Haltenbanken, near the coast of Norway, was obtained from the IAHR working group on extreme waves. The chosen buoys and their locations are shown in Fig. 1. Identification codes, regional and geographical location, measurement periods and total number of years covered by the data for each buoy are given in Table 1.

Buoy measurements of H_s were prepared according to the IAHR recommended practice. Since the measurement period covered by data from the NDBC/NOAA buoys much exceeded the period covered by the altimeter database, two subsets from these buoys were created to assess the sensitivity of estimated extremes to the length of the originating database of measured H_s. The first subset consisted of all available data from each buoy within the corresponding measurement period indicated in Table 1. The second subset included data truncated to the period covered by the altimeter database (1986–1995). H_s maxima were selected from these two subsets using the POT method. The number of POT points was chosen to closely match the number of storms at each buoy location, which was estimated from a storm database described in Ref. [10]. This approach was considered convenient for automation of procedures having in mind the need of applying identical techniques for the intended global analysis of extreme H_s. To ensure independence of the data, consecutive H_s exceeding the chosen threshold wave height were required to be separated by time lags greater or equal to 72 h.

Extreme H_s with a 100-year return period (henceforth H_s100) were estimated through an extrapolation of the three-Parameter Weibull distribution at the appropriate probability level, with parameters fitted to the data by maximum likelihood. The three-Parameter Weibull distribution (henceforth 3PW) is given by:

$$\hat{F}(h_i) = 1 - \exp\left[-\left(\frac{h_i - a_w}{b_w}\right)k_w\right] \quad (1)$$

where h is the independent variable (significant wave height) and a_w, b_w and k_w are the location, scale and shape parameters, respectively. The distribution function $F(h_i)$, which represents the probability of non-exceedence of h, is equal to zero whenever $h_i < a$.

The differences between buoy-derived H_s100 calculated from the two subsets described above at each site were all smaller than 10% (under 5% in all but one case). This was an encouraging result, as it indicated that the shorter time length of the altimeter database could, in principle, provide consistent estimates of H_s100. It also reassured us in using the data available from the eleventh buoy, Haltenbanken, despite its shorter coverage period relative to other buoy sites. Finally, we assumed that the estimates of H_s100 made using the entire measurement period at each buoy were representative of the true H_s100. These values, which are given in Table 2, were thus taken as the target for the purposes of validation of satellite-based H_s100.

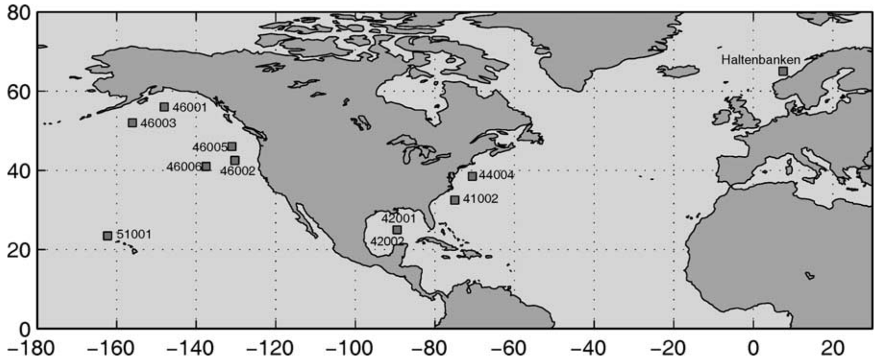

Fig. 1. Location of selected buoys: 41002, 42001, 42002, 44004, 46001, 46002, 46003, 46005, 46006, 51001 and Haltenbanken.

Table 1
Identification codes, nominal and geographical location, measurement periods and total number of years covered by the data from ocean surface buoys used in our study

Buoy	Region	Location (mean)	Measurement period	No of years
41002	SW North Atlantic	32.3°N, 75.3°W	1976–1998	22
42001	Gulf of Mexico	25.9°N, 89.7°W	1976–1998	22
42002	Gulf of Mexico	26.0°N, 93.5°W	1976–1997	21
44004	SW North Atlantic	38.6°N, 70.5°W	1977–1998	21
46001	Gulf of Alaska	56.2°N, 148.1°W	1976–1998	22
46002	NE North Pacific	42.5°N, 130.2°W	1976–1998	22
46003	Aleutian Islands	51.9°N, 155.8°W	1976–1998	22
46005	NE North Pacific	46.1°N, 131.0°W	1976–1998	22
46006	NE North Pacific	40.8°N, 137.6°W	1977–1998	21
51001	Hawaiian Islands	23.4°N, 162.3°W	1981–1998	17
Hbken	North Sea	65.1°N, 7.3°E	1980–1988	8

The IAHR procedure was then used to obtain estimates of H_s100 using altimeter data from $2° \times 2°$ and $4° \times 4°$ mesh elements centered at each buoy site. We also examined a simple alternative method to estimate H_s100 using the altimeter database, which consisted of extrapolating a Fisher-Tippet type 1 distribution fitted by maximum likelihood to data selected using the IDM. Following Carter [3], IDM data points consisted of the calculated median value of observations from each individual satellite pass within $2° \times 2°$ ($4° \times 4°$) mesh elements. This approach was also tested to verify if weighting the IDM data to compensate for undersampling affected the estimates of H_s100, as discussed in Section 5.

The Fisher-Tippet type 1 distribution (henceforth FT1) is given by:

$$\hat{F}(h_i) = \exp\left[-\exp\left(-\frac{h_i - a_f}{b_f}\right)\right], \qquad (2)$$

where a_f and b_f are the location and scale parameters, respectively.

Following Goda and Mathisen et al. [13,19], values of H_s100 estimated from POT data were associated with a probability level given by $P(H_s < H_s100) = 1 - N_Y/(100N_{POT})$, where N_{POT} is the number of selected POT points and N_Y is the number of years covered by the POT series. In the case of IDM data, values of H_s100 were estimated by extrapolating the chosen distribution functions to a probability level given by $P(H_s < H_s100) = 1 - D/T_{100}$, where D is a decorrelation time scale in hours for observations of H_s and T_{100} is the number of hours in 100 years. Consistent with the decorrelation time scales for H_s used in other studies [9,25,27], we chose $D = 3$ h.

Confidence intervals for all estimates of H_s100 were calculated using empirical formulae proposed by Goda [13] for the 3PW and the FT1 distributions. The goodness of fit of statistical distributions to series of H_s maxima were measured in terms of the Cramer Von Mises test (C), a modified Kolmogorov–Smirnov test (T) proposed in Ref. [8], for when distribution parameters are estimated from the data, and a criterion based on the correlation coefficient (R) proposed by Goda and Kobune [14]. Failures and passes were determined considering a 95% confidence level.

5. Results

Results are presented in two subsections dedicated to (i) the validation of H_s100 relative to reference values estimated from buoy data and (ii) the results of applying two methodologies for computing global estimates of H_s100 using the combined altimeter database. In Section 5.1 we also examine some issues related to undersampling and to seasonal observation bias in satellite observations of H_s, focusing on their consequences for estimates of H_s100 and alternatives for minimizing these effects.

5.1. Satellite- vs. buoy-derived H_s100

Table 3 summarizes the estimates of H_s100 made using $2° \times 2°$ altimeter data and three alternative

Table 2
Estimates of H_s100 made using buoy data and the IAHR recommended practice

Buoy	H_s100 (m) IAHR/buoy	N_P	C/R/T
41002	12.83 ± 2.15	244	P/P/P
42001	9.08 ± 1.50	246	F/P/F
42002	8.70 ± 1.30	237	F/P/P
44004	12.94 ± 1.63	250	P/P/P
46001	15.74 ± 1.81	476	P/P/P
46002	15.85 ± 2.14	247	P/P/P
46003	17.89 ± 2.53	357	P/P/P
46005	15.05 ± 1.76	266	P/P/P
46006	15.86 ± 2.05	229	P/P/P
51001	11.55 ± 1.57	186	F/P/P
Hbken	14.95 ± 1.56	118	P/P/P

Also indicated are the confidence intervals, the number of POT points N_P and scores for goodness of fit in terms of the following tests: Cramer Von Mises test (C), Kolmogorov–Smirnov (T) and the REC criterion (R) of Goda and Kobune [14]. Failures (F) and passes (P) are given at a 95% confidence level.

Table 3
Estimates of H_s100 made using 2° × 2° altimeter data and the IAHR recommended practice (IAHR), the FT1 model with IDM data (FT1) and the weighted FT1 model (WFT1)

Site	H_s100 (m) IAHR/alt	N_P	C/R/T	$\Delta\%$	H_s100 (m) FT1/alt	N_I	C/R/T	($\Delta\%$)	H_s100 (m) WFT1/alt	N_I	C/R/T	$\Delta\%$
41002	13.52 ± 6.25	98	F/P/P	5.38	11.66 ± 1.08	464	F/P/F	−9.12	13.67 ± 1.08	464	F/P/F	6.53
42001	8.22 ± 2.90	122	F/P/P	−9.39	8.58 ± 0.68	412	P/P/P	−5.42	8.87 ± 0.68	412	F/P/F	−2.22
42002	5.50 ± 0.92	128	P/P/P	−36.83	7.78 ± 0.61	435	P/P/P	−10.58	8.38 ± 0.61	435	F/P/F	−3.62
44004	13.05 ± 4.31	109	P/P/P	0.81	14.63 ± 1.24	575	F/P/F	13.02	13.25 ± 1.24	575	F/F/F	2.33
46001	11.86 ± 2.52	258	F/P/P	−24.64	15.79 ± 1.41	830	F/P/P	0.27	16.20 ± 1.41	830	F/P/P	2.92
46002	10.25 ± 1.76	106	P/P/P	−35.30	15.12 ± 1.15	671	F/P/F	−4.59	15.07 ± 1.15	671	F/P/F	−4.91
46003	13.38 ± 2.20	188	F/P/P	−25.19	18.24 ± 1.45	842	P/P/P	1.95	17.74 ± 1.45	842	F/P/F	−0.82
46005	12.15 ± 2.12	133	F/P/P	−19.23	15.93 ± 1.24	757	F/P/F	5.89	15.92 ± 1.24	757	F/P/F	5.80
46006	12.79 ± 2.47	99	P/P/P	−19.38	16.55 ± 1.33	561	F/P/P	4.35	17.17 ± 1.33	561	F/P/P	8.26
51001	8.33 ± 2.39	108	F/P/P	−27.89	9.82 ± 0.69	582	P/P/P	−14.96	10.05 ± 0.69	582	P/P/P	−12.98
Hbken	13.17 ± 3.91	150	P/P/P	−11.91	17.34 ± 1.49	261	F/P/P	15.99	17.20 ± 1.49	261	F/P/P	15.01
$\overline{\lvert\Delta\%\rvert}$				19.63				7.83				7.39
$\overline{\Delta\%}$				−18.51				−0.29				1.48

Also indicated are the percentage bias of altimeter H_s100 relative to the buoy-derived estimates ($\Delta\%$), the mean bias $\overline{\Delta\%}$ and the mean absolute bias ($\overline{\lvert\Delta\%\rvert}$). A definition of other indicated parameters is given in Table 2.

statistical extrapolation methods based on: the IAHR recommended practice, the FT1 model using IDM data and a variation of this latter technique using a weighted method of moments for estimation of distribution parameters. These several altimeter-based estimates of H_s100 and their associated confidence intervals are compared to buoy-IAHR H_s100 in Fig. 2. Table 3 also indicates the percentage bias of the estimates of altimeter H_s100 relative to the buoy-IAHR H_s100 given in Table 2.

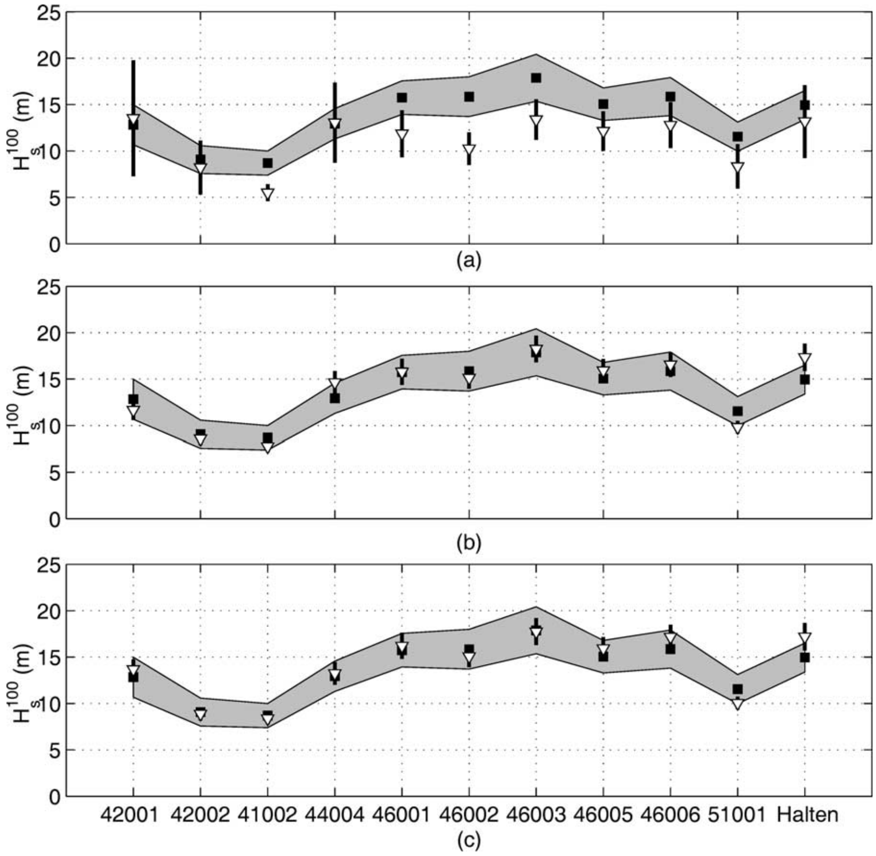

Fig. 2. 2° × 2° Estimates of H_s100 made with buoy data using the IAHR recommended practice are indicated in all panels by squares. Associated 95% confidence intervals are indicated by the shaded regions. Triangles indicate estimates of H_s100 made with altimeter data using (a) the IAHR recommended practice, (b) the FT1 distribution with IDM data using the method of moments (MOM) and (c) the FT1 distribution with IDM data using a weighted method of moments (WMOM). The 95% confidence limits for the altimeter results are shown by the vertical solid lines.

A comparison of H_s100 estimated using buoy and altimeter data and the IAHR recommended practice is presented in Fig. 2(a). This figure shows that the altimeter-IAHR H_s100 generally underestimates the buoy values, with most altimeter-based estimates falling below the 95% confidence intervals of buoy estimates. This is consistent with the large negative values for relative bias seen in Table 3. The differences between buoy and altimeter-IAHR H_s100 were generally larger at buoys located in the higher latitudes of both the North Atlantic and the North Pacific oceans (from around −20 to −35%), although the largest bias (−38.83%) was associated with buoy 42002, in the Gulf of Mexico. The mean absolute bias was 19.63%.

We note that despite these large discrepancies between buoy and satellite estimates of H_s100, the results for goodness of fit given in Table 3 indicate that the 3PW distribution fits successfully the POT maxima from both buoy and altimeter data in the vast majority of locations. On the other hand, this may be a result of the relatively small number of POT points used in parameter fitting, which allow broader tolerance limits at a given statistical confidence level relative to cases using IDM data (see below).

Altimeter-based estimates of H_s100 made using the FT1 distribution and IDM data, on the other hand, agreed remarkably well with the buoy-IAHR H_s100. This good agreement is clearly verified in Fig. 2(b), which also shows that most altimeter-based estimates of H_s100 fell within the 95% confidence intervals associated with buoy-IAHR H_s100. Again, the larger discrepancies of satellite H_s100 relative to buoy estimates were observed in the higher latitudes of both the North Atlantic and the North Pacific Oceans (from around 10 to 15%). The mean absolute bias was 7.83%.

Despite the good match between the altimeter-FT1 H_s100 and the buoy-IAHR estimates, goodness-of-fit criteria indicated that the FT1 model does not provide a good description of IDM data from the combined altimeter database in nearly half of the buoy locations, contrasting the generally good fit of the 3PW model to POT data in most validation sites. This, however, may be due to the fact that the much larger number of data points used in the IDM, relative to POT data, leads to relatively narrower tolerance limits at a given statistical confidence level. This, in turn, may explain the larger number of failures associated with the FT1 model. Support for this idea is provided by Fig. 3, which shows empirical and model CDFs associated with buoy 46006, in the NE North Pacific. This figure indicates that both statistical models seem to provide a visually acceptable fit to both POT and IDM data.

In objective terms, it is only possible to say that goodness-of-fit tests applied to our results and evidence presented in previous studies [15,19,28] seem to indicate that the FT1 model is not as appropriate as the 3PW model for estimating extreme H_s. On the other hand, the results above reveal large discrepancies between buoy- and satellite-IAHR (3PW) H_s100, indicating differences between altimeter data and in situ measurements that are significant for estimating extreme H_s. Our results also show that these discrepancies are significantly reduced when estimates of H_s100 made using altimeter data are obtained with a FT1 distribution fitted to IDM data.

The fact that a series of altimeter H_s maxima, selected using the POT method to represent storm events, provides estimates of H_s100 that systematically underestimate the target buoy-derived H_s100, suggests that some degree of undersampling of storm maxima by altimeters on board Earth-orbiting satellites is occurring. Support for this hypothesis is provided in Fig. 4(a), which shows a scatter-plot of co-located satellite- and buoy-derived monthly H_s maxima at selected validation sites. This figure reveals that monthly H_s maxima extracted from the altimeter database systematically underestimate the corresponding monthly buoy maxima, thus indicating that the satellite measurements missed or misrepresented a significant number of severe sea states during the period covered by the combined altimeter database. This issue and its effects on the altimeter-IAHR estimates of H_s100 are examined next.

5.1.1. Satellite undersampling and POT data

Several factors may cause altimeters on board satellites to undersample storm H_s. The most conspicuous is the satellite orbital cycle, which determines the time interval between two consecutive passes over the same point (i.e. the sampling rate). Two other important factors are the geometrical properties of the orbit and the development of gaps during certain periods of time or at particular locations. The first factor leads to different spatial coverage or resolution of the ocean surface as a function of geographical location. The second factor arises as a consequence of characteristics of satellite missions, malfunctioning or spurious radar returns due to proximity of land or other obstacles, such as pack ice. The effects of gaps in the available time series will be examined in a following subsection. In this subsection we examine the undersampling resulting from the satellite orbital cycle and its effects on estimates of H_s100 made using the IAHR recommended practice.

We begin by estimating the average sampling intervals associated with the merged database of altimeter measurements used presently, defined as the mean time between consecutive passes within $2° \times 2°$ mesh elements centered at NODC/NOAA buoy sites. These average sampling intervals are as follows: 71 h at 41002, 71 h at 42001, 72 h at 42002, 57 h at 44004, 56 h at 46001, 69 h at 46002, 56 h at 46003, 56 h at 46005 and 69 h at 51001. These values reflect a global average of all satellite missions. Furthermore, they represent the time interval between consecutive satellite passes over any point within a mesh element, which is consistent with the assumption that measurements made anywhere within a mesh element are representative of

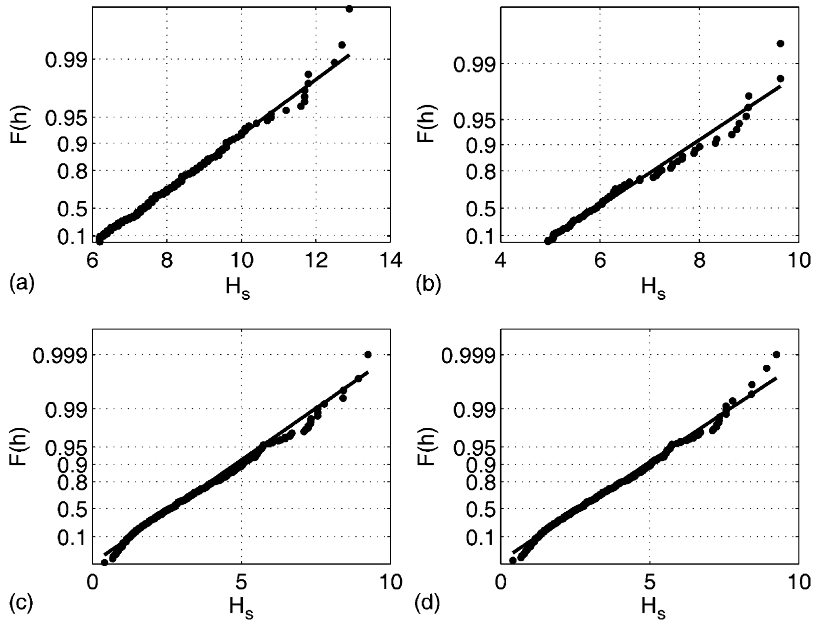

Fig. 3. Diagram showing observations (black circles) and model estimates (continuous lines) of the distribution function $F(h_i)$, i.e. the probability of non-exceedence of h, against values of H_s at buoy 46006, as follows: (a) 3PW model fitted to buoy-POT data using maximum likelihood, (b) 3PW model fitted to altimeter-POT data using maximum likelihood, (c) FT1 model fitted to IDM data using maximum likelihood and (d) FT1 model fitted to IDM data using a weighted method of moments.

the center-point. Therefore, the average sampling intervals mentioned here should not be mistaken for the repeat or revisit time interval of the satellite footprint over any given point, which is of the order of four to eight times larger.

A global view of sampling averages in hours is provided in Fig. 5, which also gives an impression of the spatial coverage of data from the combined altimeter database (higher pass densities are found along preferential tracks of the three satellite missions). Regions of higher pass density occur in higher latitudes and are, therefore, associated with higher spatial resolution relative to areas near the Equator. This zonal dependence of sampling intervals and, consequently, of spatial resolutions may seem a problem in a global climatology of extreme H_s, which may also have been amplified by the use of a grid consisting of regular mesh elements. Fig. 5 reflects the overall density of satellite passes within mesh elements for the combined database. A mission-specific description of track density and spatial resolution may be found in Refs. [7,11,12] for Geosat, ERS-1 and Topex/Poseidon, respectively.

Nevertheless, some investigations [16,26] support the idea that, on a global scale, the wave climate has larger decorrelation scales near the Equator, which is significantly reduced toward higher latitudes. We assume presently that this effect counteracts the zonal dependence of sampling intervals seen in Fig. 5, noting that biases of altimeter-derived H_s100 computed so far do not seem to reflect any dependence on latitude. Although this assumption may be reasonable for the present analysis, which focuses on the climatology of extremes on a global scale, some potential limitations in terms of impacts on local wave climatology of extremes warrant further research.

These average sampling intervals are clearly much larger than the common measurement intervals of in situ buoy data, typically 1 or 3 h. To investigate how these long sampling intervals affect the estimation of extreme H_s, buoy data were resampled at times corresponding to ± 30 min from satellite passes within $2° \times 2°$ mesh elements centered at each buoy location. These resampled, co-located data were then used to provide estimates of IAHR H_s100.

Results are summarized in Table 4, which also indicates the bias of resampled buoy-IAHR H_s100 to the target values ($\Delta_B\%$) from Table 2 and to the altimeter-IAHR $H_s100(\Delta_S\%)$ from Table 3. The impact of resampling buoy data at times co-located with measurements from the altimeter database is dramatic. The bias of H_s100 calculated from resampled buoy data indicates a systematic

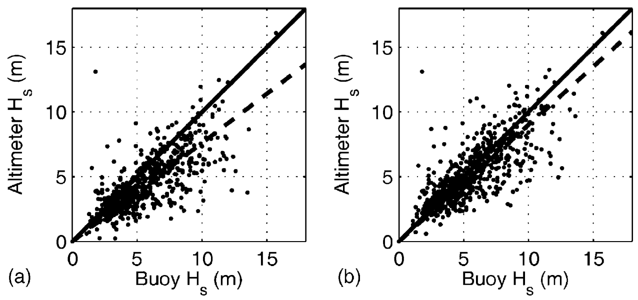

Fig. 4. Scatterplot of monthly maximum H_s values from the combined satellite altimeter database (Altimeter H_s) against in situ observations (Buoy H_s) at 10 NOAA deep water buoy locations. Results for (a) $2° \times 2°$ and (b) $4° \times 4°$ mesh elements are shown.

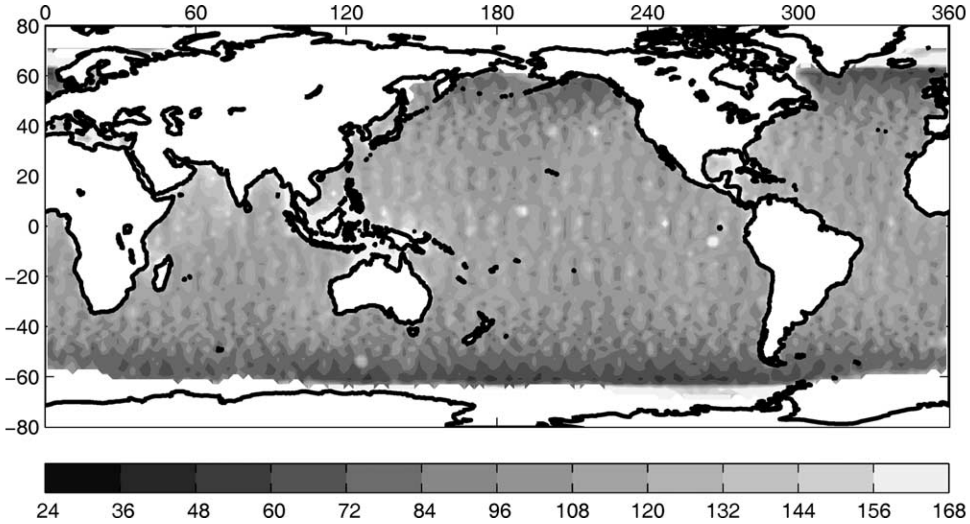

Fig. 5. Global plot of satellite pass densities in hours at 2° × 2° mesh elements. The shaded values represent the average time (hours) between satellite passes.

underestimation of 30.50% relative to the original buoy-IAHR H_s100. On the other hand, altimeter-IAHR H_s100 are now closer to resampled buoy-IAHR H_s100 than to the original buoy-IAHR H_s100 estimates, as indicated by a mean absolute bias of 13.37%.

It is also noteworthy that the largest discrepancies between resampled buoy-derived H_s100 and satellite-derived estimates (around 20%) now occur at buoy locations exposed to both mid-latitude storms and hurricanes, in the Gulf of Mexico (buoys 42001 and 42002) and near the east coast of the United States (buoys 41002 and 44004). Estimates of H_s100 made with resampled data from buoys located in the Pacific Ocean, which are usually exposed only to mid-latitude storms, have smaller discrepancies.

A closer look at time-series of measured H_s allows the identification of possible causes for these larger discrepancies between satellite-derived H_s100 and estimates made with resampled buoy data in areas exposed to hurricanes. Fig. 6 shows segments of hourly buoy measurements of H_s, along with co-located resampled-buoy and satellite observations made at buoys 41002, 42001 and 42002. Fig. 6(a) illustrates a case in which both satellite and buoy sampled maximum waves associated with the event that became knows as the 'storm of the century'. This event developed after wind fields from a hurricane and from an extratropical storm collided, generating extreme winds and waves around March 14th 1993 near NDBC buoy 42001.

Situations in which the highest of all significant wave heights associated with an extreme event are captured fully are relatively rare, because extreme events tend to be short-lived and highly localized in a relatively small spatial domain. Consequently, more often the most severe conditions are missed altogether by buoys and/or satellite-borne devices alike. An example of the latter in which altimeter measurements missed the highest waves from a severe sea-state event recorded by buoy data is shown in Fig. 6(b). Peak waves recorded by NDBC buoy 42002 in this event were generated during hurricane Gilbert's passage through the Gulf of Mexico on September 1988. Note that when buoy data are resampled at the average altimeter pass time the peak waves are also not recorded. In Fig. 6(c) the reverse situation is illustrated. The highest waves generated by hurricane Allison near NDBC buoy 42001 on June 1995 in the Gulf of Mexico, were well captured in the altimeter data series and almost completely missed by both hourly and resampled buoy data.

Other than the straightforward conclusion that satellite observations undersample H_s relative to hourly buoy data, as a consequence of the large time lags between passes occurring from the satellite's orbital cycle, Fig. 6 shows that on some occasions the satellite captures intense storms that are not recorded accurately in buoy data. This problem was often intensified by increasing the buoy sampling interval to match mean altimeter sampling intervals. As noted in previous studies [9,26], the larger area swept by the orbiting

Table 4
Estimates of IAHR (3PW) H_s100 made using buoy data co-located in time with altimeter observations centered at each buoy site

Buoy	H_s100 (m) IAHR/buoy	N_P	C/R/T	Δ_B%	Δ_S%
41002	10.59 ± 5.05	101	F/P/P	−17.42	−21.04
42001	5.82 ± 1.47	126	F/P/F	−35.88	−29.17
42002	4.39 ± 1.19	128	P/P/P	−49.55	−20.20
440044	10.86 ± 2.80	115	P/P/P	−16.11	−16.81
46001	11.20 ± 1.74	249	P/P/P	−28.5	−5.58
46002	10.21 ± 2.10	118	F/P/P	−35.55	−0.34
46003	14.10 ± 2.89	175	P/P/P	−21.19	5.38
46005	10.62 ± 3.11	139	F/P/P	−29.47	−12.63
46006	10.66 ± 3.09	116	P/P/P	−32.78	−16.65
51001	7.14 ± 1.51	111	F/P/P	−38.16	−14.26
$\overline{\lvert\Delta\%\rvert}$				30.50	13.37
$\overline{\Delta\%}$				−30.50	−12.29

The last two columns of this table indicate the bias of resampled buoy-IAHR H_s100 to the target buoy-IAHR values (Δ_B%) and to the altimeter-IAHR $H_s100(\Delta_S\%)$. A description of other associated parameters is given in Tables 2 and 3.

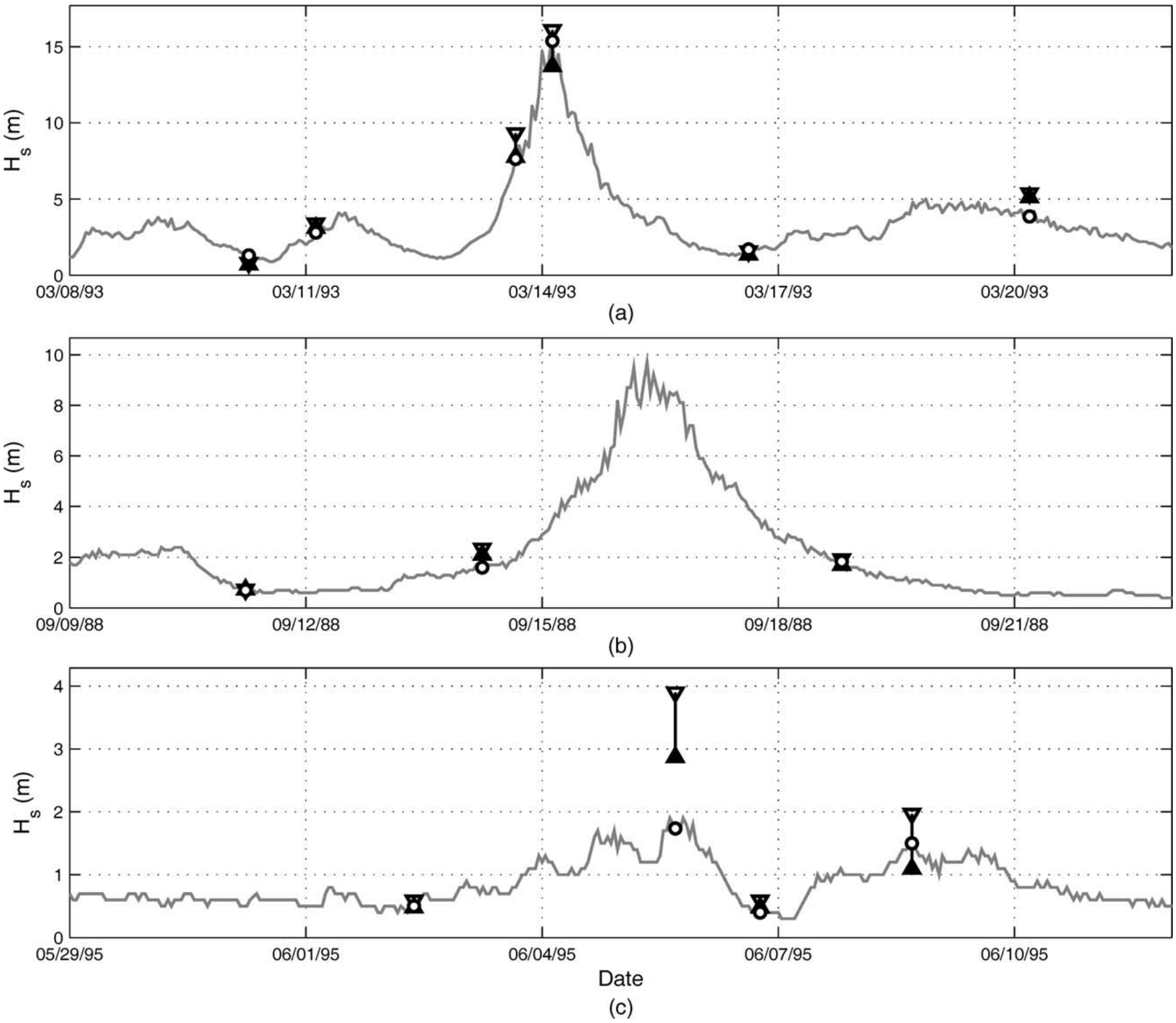

Fig. 6. Time series of H_s measured during (a) the 'storm of the century' at buoy 42001, (b) hurricane Gilbert at buoy 42002 and (c) hurricane Allison near buoy 42001. In panel (a) both satellite and buoy made consistent samples of maximum waves associated with the event. Panel (b) shows a case in which the altimeter missed the storm peak, whereas panel (c) shows a case in which buoy measurements underestimated significantly the maximum waves sampled by the altimeter. Hourly buoy data appear as continuous lines; symbols represent median (▲) and maximum (▽) altimeter values and buoy values resampled at the mean altimeter track time (○).

satellite is more effective than the single-point buoy observations in capturing some storm events, in this special case in which buoy and altimeter sampling rates are comparable. This 'compensation effect' explains the larger discrepancies of resampled buoy data seen in Table 4.

Although somewhat beneficial, the larger spatial coverage is not enough to overcome storm undersampling by the satellite-borne altimeter and its effects on estimating H_s100. In other words: these results indicate that the sampling rate is critical given the temporal and spatial scales of orbital cycles from satellite missions considered presently. Consequently, satellite-derived H_s100 estimated using POT data and the 3PW distribution are negatively biased relative to estimates made from hourly buoy data. These roles are inverted by resampling buoy data at times co-located with the times of the satellite within a $2° \times 2°$ mesh element around the buoy site. Most estimates of H_s100 made with resampled buoy observations using POT data and the 3PW model present a negative bias relative to altimeter-derived IAHR/POT H_s100. This is a likely consequence of the larger spatial coverage of satellite track relative to the single-point buoy observation, as supported by Fig. 6.

The spatial compensation for time undersampling in satellite observations seems less effective for the purposes of estimating H_s100 in areas exposed to both extratropical and tropical storms relative to areas where only extra-tropical storms occur. There are at least two reasons for this. One is that the difference between average and storm H_s values in areas exposed only to extratropical storm events is not as large as this relative difference when areas exposed to tropical storms or hurricanes are considered. Consequently, the undersampling of storms has a relatively larger impact in areas exposed to hurricanes.

The second reason for a greater effectiveness of this spatial compensation in areas exposed only to extratropical storms has to do with the relatively larger size of these storms. Typical sizes of wave-generating wind fields in extratropical storms are of the order of magnitude of the $2° \times 2°$ mesh elements. Hence, the probability that both co-located buoy and satellite data will capture the same event is high. Also, since the satellite will sample across a larger area, the chances that it will capture the sector with stronger winds and higher waves is also greater. Therefore, satellite-derived H_s100 will tend to be less-biased than estimates made with resampled buoy data, as seen in Table 4.

This effect is even greater in areas exposed to tropical storms or hurricanes, which have sizes typically of the order of tens of kilometers. In this case, not only will the satellite track have a larger chance of recording the highest waves sector, but it will capture storms that are completely missed not only by the point-resampled buoy data, but even by hourly buoy records, as seen in Fig. 6(c). This explains why the estimates of H_s100 made with resampled buoy data discussed previously present a larger negative bias relative to hourly-buoy-derived H_s100 than the altimeter-derived estimates of H_s100.

The empirical evidence presented in this section indicates that the superior spatial coverage of satellite measurements relative to point in situ observations partly compensates for time undersampling resulting from properties inherent to satellite orbital cycles. Although this provides some insight into the nature of measurements made by satellite altimeters, from the practical point of view, temporal undersampling is still a predominant source of error for the purposes of calculating H_s100 using the POT method. This leads to POT-based estimates of extreme values that are generally much smaller than those obtained using hourly buoy data. A potential alternative to reduce this effect by using data from larger, $4° \times 4°$ mesh elements is examined in the next section.

5.1.2. Altimeter data from 4° × 4° mesh elements

The effect of increasing the satellite database mesh element size to areas covering $4° \times 4°$ in latitude and longitude is illustrated in Fig. 4(b), which presents a scatterplot of monthly altimeter-derived H_s maxima against buoy-derived monthly maxima. A comparison of this figure with Fig. 4(a) suggests that these larger mesh elements provide series of altimeter-derived monthly H_s maxima that are more consistent with buoy data.

We may speculate that estimates of H_s100 with reduced bias may also be obtained by using larger $4° \times 4°$ mesh elements. This approach, however, may have a drawback, since the expanded area relative to $2° \times 2°$ mesh elements may be so large that observations belonging to areas with different wave climatology are combined into time series that should be representative of the same point. This, in turn, would compromise the statistical reliability of estimated H_s100. To examine more closely these issues we compare estimates of H_s100 made from altimeter data extracted from $4° \times 4°$ mesh elements with the buoy-derived IAHR H_s100 from Table 2. Statistical reliability of these new estimates of H_s100 is measured in terms of the three goodness-of-fit tests previously defined. Results of this comparison are presented in Table 5.

A comparison between Tables 3 and 5 reveals that the larger mesh elements had little overall impact on estimates of H_s100 made using IDM data and the FT1 distribution, except for a poorer performance of $4° \times 4°$ elements in terms of goodness-of-fit scores. On the other hand, the bias of estimates made with POT data and the 3PW distribution was significantly reduced, whereas the statistical reliability of these new estimates remained unchanged. This improvement in estimates of H_s100 made with POT data is illustrated in Fig. 7, which should be compared to Fig. 2(a). FT1 model

Table 5
Estimates of H_s100 made using $4° \times 4°$ altimeter data

Site	H_s100 (m) IAHR/alt	N_P	C/R/T	$\Delta\%$	H_s100 (m) FT1/alt	N_I	C/R/T	$\Delta\%$	H_s100 (m) WFT1/alt	N_I	C/R/T	$\Delta\%$
41002	15.81 ± 5.53	104	F/P/P	23.20	10.74 ± 0.97	970	F/P/F	−16.33	12.21 ± 0.97	970	F/P/F	−4.88
42001	8.60 ± 3.42	125	F/P/F	−5.26	8.07 ± 0.62	811	F/P/F	−11.10	8.20 ± 0.62	811	F/P/F	−9.65
42002	7.04 ± 1.24	116	P/P/P	−19.02	8.09 ± 0.60	882	F/P/F	−7.00	8.21 ± 0.60	882	F/P/P	−5.61
44004	14.95 ± 2.96	123	P/P/P	15.53	13.20 ± 1.17	1069	F/F/F	1.96	14.23 ± 1.17	1069	F/F/F	9.97
46001	13.85 ± 2.42	234	F/P/P	−12.05	15.87 ± 1.34	1779	F/P/F	0.81	15.75 ± 1.34	1779	F/P/F	0.04
46002	10.83 ± 1.49	125	P/P/P	−31.66	14.91 ± 1.14	1269	F/P/F	−5.89	15.21 ± 1.14	1269	F/P/F	−4.01
46003	15.00 ± 2.33	185	P/P/P	−16.13	17.82 ± 1.44	1528	F/P/P	−0.36	17.78 ± 1.44	1528	F/P/F	−0.61
46005	13.46 ± 2.27	138	F/P/P	−10.56	16.05 ± 1.24	1471	F/P/F	6.68	16.25 ± 1.24	1471	F/P/F	7.97
46006	13.02 ± 2.06	129	P/P/P	−7.91	16.77 ± 1.32	1177	F/P/F	5.68	17.18 ± 1.32	1177	F/P/F	8.32
51001	9.41 ± 1.44	125	F/P/P	−18.51	10.05 ± 0.72	1212	P/P/P	−12.93	10.30 ± 0.72	1213	F/P/P	−10.82
Hbken	13.74 ± 2.25	141	P/P/P	−8.11	16.89 ± 1.43	446	F/P/P	12.98	17.55 ± 1.43	446	F/P/F	17.36
$\overline{\lvert\Delta\%\rvert}$				16.18				7.43				7.20
$\overline{\Delta\%}$				−9.13				−2.32				0.73

A description of other indicated parameters is given in Tables 2 and 3.

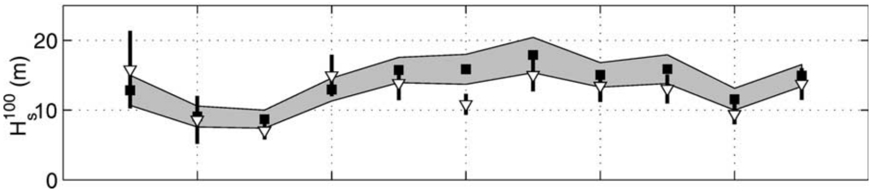

Fig. 7. Estimates of H_s100 made with data from $4° \times 4°$ mesh elements. Shown are values computed using buoy data and the IAHR recommended practice (squares) with associated 95% confidence intervals (shaded regions) and estimates of H_s100 made with altimeter data using the IAHR recommended practice (triangles).

estimates were not included in Fig. 7 as they were nearly identical to those plotted in Fig. 2(b) and (c).

Parameters of the FT1 model are estimated to provide a best fit to IDM data, i.e. the entire collection of measurements made at a particular location. An initial assessment of how the properties of IDM data from $2° \times 2°$ and $4° \times 4°$ mesh elements differ may be made by testing their statistical equivalence. Using a two-sample t-test [22] we conclude that the two samples are statistically equivalent at a 90% confidence level. This equivalence is illustrated in Fig. 8, which shows a scatter-plot of monthly mean H_s derived from $2° \times 2°$ and $4° \times 4°$ mesh elements.

Tables 3 and 5 reveal that estimates of H_s100 made using POT data extracted from $4° \times 4°$ mesh elements are, in all cases, higher than H_s100 computed using $2° \times 2°$ data. As discussed previously, Fig. 4 indicates that increasing the mesh-element size also increases the chances of the satellite track encountering a larger number of storms and/or storm sectors of stronger winds not 'seen' by $2° \times 2°$ mesh elements. Consequently, estimates of H_s100 made using POT data from $4° \times 4°$ mesh elements are relatively higher and closer to the target buoy-derived IAHR/POT H_s100.

Results presented in this section indicate that an increase in the mesh-element size from $2° \times 2°$ sectors to $4° \times 4°$ may be beneficial to the estimation of H_s100 using POT data and the 3PW distribution. However, the increased mesh-element size had little or no impact on estimates of H_s100 made using IDM data and the FT1 model. Considering the positive impact to the former, our global analysis of H_s100, presented below, is based on outcomes from databases composed of both $2° \times 2°$ and $4° \times 4°$ mesh elements. Before advancing that far, we examine next the effects of the 'seasonal' signal in the altimeter data, on the estimates of H_s100.

5.1.3. Weighted FT1

Seasonal fluctuations in the number of satellite passes per month (monthly measurement density) within mesh elements of the altimeter database may affect the estimates of H_s100, particularly when IDM data are used. These seasonal fluctuations result from a combination of factors inherent to satellite missions, such as periods of malfunctioning or maneuvering and, more importantly, the time of year in which these satellite missions were initiated and concluded. Coincidentally, Geosat observations became available on December 1986, while ERS-1 data were collected from August 1991 and TOPEX/Poseidon measurements were obtained from November 1992. The combination of the three data sets resulted in a greater proportion of observations being made during the northern hemisphere winter. This is illustrated in Table 6, which shows the monthly measurement densities of the altimeter database at selected buoys sites.

The effects of non-uniform distribution of passes may be reduced by extending the database to include earlier Geosat data recently made available and ERS-2, TOPEX/Poseidon and data from other altimeter-carrying satellites collected since 1995. However, this larger database is not yet available. Therefore, we assess the impact of this limitation to estimates of H_s100 made using the combined database presently available using a simple but effective approach to reduce the non-uniform monthly measurement density. Following Carter [3], this approach consisted of recalculating the parameters of the FT1 distribution using a weighted method of moments (henceforth WFT1), which is based on the following two steps:

1. Eliminate the non-uniform distribution by recomputing the sample mean and variance, as follows:

$$\hat{\mu} = \frac{\sum p_i/n_i}{12} \qquad (3)$$
$$\hat{\sigma} = \frac{\sum q_i/n_i}{12} - \hat{\mu}^2$$

   where p is the sum of H_s, q is the sum of squares of H_s and n is the number of observations within each month $i = [1, 12]$.
2. Recalculate a_f and b_f, the location and scale parameters of the FT1 distribution (Eq. (2)), using the following

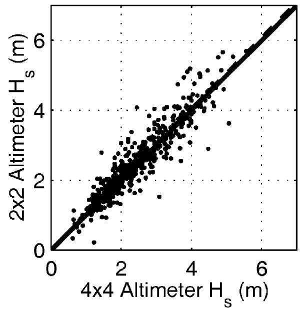

Fig. 8. Scatterplot of monthly mean satellite observations of H_s comparing data from $2° \times 2°$ and $4° \times 4°$ mesh elements.

Table 6
Density of satellite passes throughout the year at each buoy location

Buoy	Jan	Feb	Mar	Apr	May	Jun	Jul	Aug	Sep	Oct	Nov	Dec
41002	35	37	38	39	38	29	28	38	35	42	51	54
42001	51	45	46	38	26	24	18	21	24	35	38	46
42002	55	47	45	41	36	26	16	26	20	31	40	42
44004	62	55	65	50	48	33	34	39	35	38	52	64
46001	70	63	67	82	76	63	65	75	57	66	66	80
46002	59	63	63	59	57	44	44	58	44	52	61	67
46003	87	84	83	81	73	58	60	65	47	60	70	74
46005	67	71	54	67	61	50	43	72	61	60	73	78
46006	43	40	38	49	52	37	41	54	46	50	53	58
51001	43	34	44	4‘5	55	39	51	63	43	51	59	55
Hbken	38	43	51	45	20	12	8	10	5	6	15	27

expressions, which equate the weighted estimates of the sample mean and variance to the population mean and variance of the FT1 model:

$$\hat{\mu} = a_f + \gamma b_f$$

$$\hat{\sigma}^2 = \frac{\pi^2 b_f^2}{6},$$

where $\gamma = 0.5772$ is the Euler number.

Estimates of H_s100 made with the WFT1 using $2^\circ \times 2^\circ$ data are presented in Table 3. Fig. 2(c) shows these estimates plotted against the buoy-derived IAHR H_s100. The WFT1 provides estimates of H_s100 that are very close to buoy-derived H_s100 (the mean absolute bias was 7.39%), repeating the agreement obtained with estimates of H_s100 made with the FT1 distribution with unweighted parameters (see Table 3). Also, in the majority of locations altimeter estimates again fell within the 95% confidence limits of buoy-derived H_s100. We conclude that both weighted and unweighted FT1 models produce estimates of H_s100 that are very similar, which confirms results previously reported by Carter [3].

Tables 3 and 5 also indicate the results of goodness-of-fit for WFT1 H_s100 based on the same tests applied to the unweighted FT1 estimates. A noticeable reduction in the number of pass levels relative to the latter is likely associated with the fact that the WFT1 model is being compared to uncorrected IDM data. Since this IDM data remains contaminated by the seasonal bias eliminated in the WFT1 model, the resulting weighted model distribution will fit less-well the biased empirical distribution when compared to the performance of the unweighted FT1 model. Consequently, whenever the WFT1 model is used, the goodness-of-fit tests chosen become useless as a statistical inference tool.

It is, thus, fortunate that the unweighted FT1 model provides estimates of H_s100 that are coherent with the unbiased WFT1 model, as they are associated with statistical models that can be assessed properly in terms of goodness-of-fit. Assuming that this coherency may be extrapolated for other sites around the globe, the next section presents an assessment of global estimates of H_s100 made with the FT1 model using the complete combined altimeter database, with data from both $2^\circ \times 2^\circ$ and $4^\circ \times 4^\circ$ mesh elements. Goodness-of-fit tests provide a statistical basis for comparison of these estimates with global values of H_s100 computed using POT data and the 3PW distribution, which are also presented below.

5.2. Global estimates of H_s100

In this section we present the results of a global analysis of extreme wave height using the database of combined Geosat, Topex/Poseidon and ERS-1 altimeter measurements of Young [29]. As mentioned above, the two techniques used in our analysis are the method recommended by the IAHR, consisting of using POT data and the 3PW model, and an approach based on the FT1 model fitted to IDM data. The choice of these two methods for our analysis of global extreme H_s is based on the results and discussions presented above.

In brief, the IAHR method was chosen because it has been proposed and used as a standard for the analysis of extremes computed using buoy data. Although our validation analysis indicated its application to altimeter data does not provide estimates of H_s100 consistent with buoy-derived extremes, it is interesting to assess its behavior on a global basis in terms of spatial coherency and statistical reliability. On the other hand, the FT1 model applied to the altimeter database delivers estimates of H_s100 that are in very good agreement with buoy-derived estimates, but have a relatively poor statistical reliability in terms of goodness-of-fit tests. Thus, it is also interesting to examine its behavior on a global basis.

Considering the validation analysis presented above, estimates of H_s100 made using POT data and the 3PW model were made with satellite observations from both $2^\circ \times 2^\circ$ and $4^\circ \times 4^\circ$ mesh elements. Global estimates of H_s100 made using IDM data and the FT1 model were also made with observations at the $2^\circ \times 2^\circ$ and $4^\circ \times 4^\circ$ resolutions. The statistical reliability of all global estimates

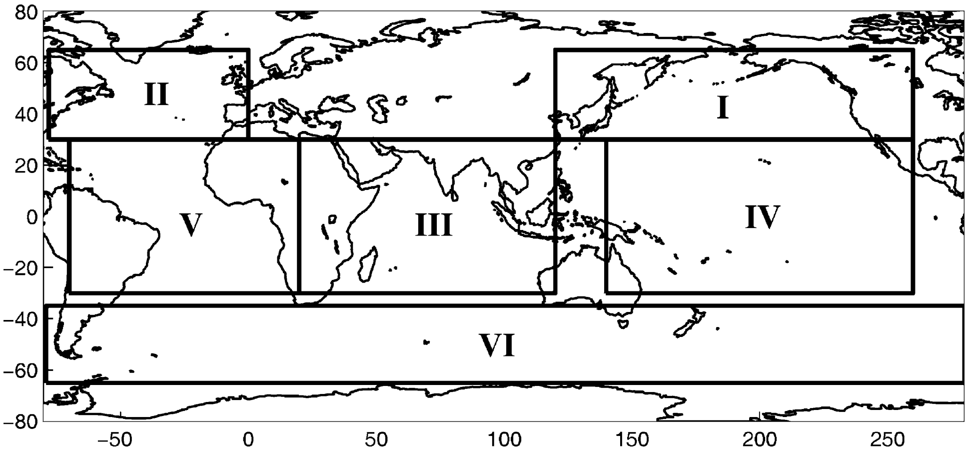

Fig. 9. Representative areas of the world's oceans used for analysis. I: Northern Pacific Ocean, II: Northern Atlantic Ocean, III: Indian Ocean, IV: Tropical Pacific Ocean, V: Tropical Atlantic Ocean, VI: Southern Ocean.

of H_s100 is assessed briefly in terms of the three goodness-of-fit tests described previously. To assist in our interpretation, the global ocean is divided in six areas as illustrated in Fig. 9.

5.2.1. POT/3PW approach

Global values of H_s100 computed using POT data from $2^\circ \times 2^\circ$ mesh-elements and the 3PW model are shown in Fig. 10. The most striking feature of this figure is a high level of spatial variability between adjacent mesh elements, which contrasts with a smooth spatial distribution of H_s100 that would be expected from a purely intuitive viewpoint. Fig. 11 shows the distribution of associated goodness-of-fit scores, which are organized into four categories based on passes or failures at the 95% confidence level of the three statistical test previously defined. These categories are: pass three tests, pass any two of three tests, fail any two tests and fail all tests.

Table 7 provides the percentage of $2^\circ \times 2^\circ$ mesh elements falling into the four score categories for goodness-of-fit mentioned above. Results are indicated for regions identified in Fig. 9. Confirming the relatively good results of the POT/3PW approach described in Section 4 in terms of the goodness-of-fit tests chosen for this study, the 3PW model seems to fit well the satellite-derived POT data in most areas, as seen in the global distribution of goodness-of-fit scores shown in Fig. 11.

Table 7 indicates that the percentage of mesh elements in which the 3PW model fit to POT data passed at least two or all three tests was over 80% in all areas. This performance was particularly good within the Indian Ocean, the Northern and Tropical Pacific and the Northern Atlantic Oceans, where the model fit passed at least two or all three tests in 90% of the cases. Slightly poorer performance was recorded in the Southern Ocean and in the Tropical Atlantic Ocean, where the percentage of points passing two or three tests was approximately 85%.

The success of the 3PW model in fitting altimeter-derived POT data in terms of the chosen goodness-of-fit tests is encouraging. However, a successful fit of a statistical

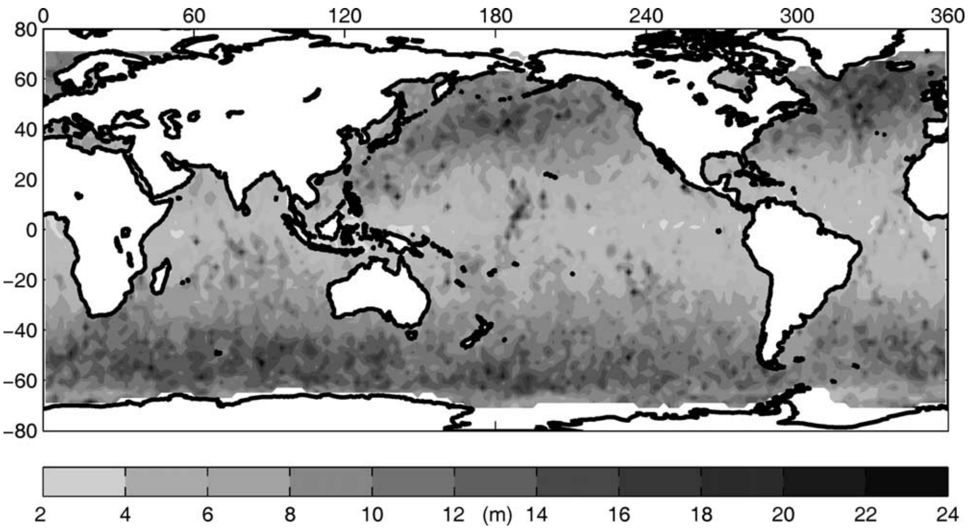

Fig. 10. Global values of H_s100 computed using POT data from $2^\circ \times 2^\circ$ mesh-elements and the 3PW model.

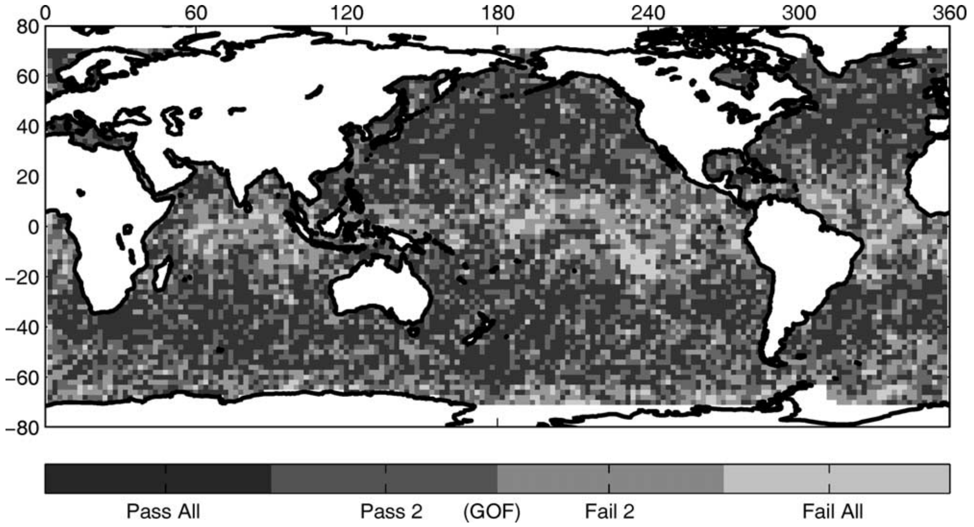

Fig. 11. Goodness of fit scores associated with the values of H_s100 of Fig. 10. The shading levels reflect the number of tests passed/failed at the 95% confidence level.

model to a chosen dataset does not necessarily represent a successful estimation of the desired parameter, as demonstrated in the validation of altimeter-derived H_s100 computed using the POT/3PW approach presented in Section 4. These validated altimeter-derived values of H_s100 were systematically lower than the associated buoy-derived target values. Thus, it is reasonable to assume that the altimeter-based global H_s100 may also be underestimations of the true values. A possible strategy to verify this assumption is to simulate the 'flight' of a satellite collecting data from long-term simulations of wave fields generated by wind-wave models, following the guidelines set by Cooper and Forristall [9], but using more sophisticated wind and wave hindcast techniques instead of simple parametric models. This is left for a future study.

A reason for greater concern is the high short-scale spatial variability of H_s100 (of the order of the $2° \times 2°$ mesh-element size) seen in Fig. 10. We examine a potential way of overcoming this intuitively-incorrect spatial distribution of H_s100 by using POT data extracted from larger, $4° \times 4°$ mesh elements. Results presented in Section 4 indicated that this may also be a potential way of obtaining estimated H_s100 in closer agreement with those obtained using in situ data. Results are shown in Fig. 12. Although the short-scale spatial variability of H_s100 is significantly reduced compared to Fig. 10, the result is still counter-intuitive. Further, Table 7 indicates that the use of data from $4° \times 4°$ mesh elements leads to a systematic increase in the percentage of locations where the 3PW fails to fit well the POT data.

Table 7 indicates that the goodness-of-fit remains fairly high (above 80% of locations passing two or three tests) in the Southern Ocean and the northern latitudes of the Pacific and Atlantic Oceans, although some reduction in performance is observed. On the other hand, the tropical regions of the Pacific and Atlantic Oceans and the Indian Ocean show a substantial decrease in performance, which is also observed in the overall scores for the entire globe.

The poorer statistical performance due to the use of larger mesh elements may be a consequence of using data from a region that is so large, that it includes observations from areas with different wave climatology. According to Tournadre [5], it is not possible to determine precisely the optimal sizes of areas within which the wave climatology

Table 7
Percentage of mesh elements satisfying each of the four categories used for assessing goodness-of-fit POT data to the 3PW model

Region	$2° \times 2°$				$4° \times 4°$			
	Pass all	Pass 2	Fail 2	Fail all	Pass all	Pass 2	Fail 2	Fail all
SO	53.2	29.5	14.9	2.4	49.0	29.1	19.1	2.8
IO	59.4	32.3	5.9	2.4	37.0	29.9	25.8	7.3
NP	75.3	19.4	4.7	0.6	63.5	25.4	9.6	1.5
TP	59.3	31.2	6.3	3.2	36.4	30.5	23.9	9.2
NA	69.8	24.5	5.4	0.3	58.5	31.4	9.1	1.0
TA	53.6	30.8	12.6	3.0	35.9	30.1	26.7	7.3
ALL	59.5	28.9	9.3	2.3	45.3	29.3	20.2	5.2

Results for $2° \times 2°$ and $4° \times 4°$ mesh elements are indicated. Regions are defined according to Fig. 9 and named as follows: Southern Ocean (SO), Indian Ocean (IO), Northern Pacific (NP), Tropical Pacific (TP), Northern Atlantic (NA), Tropical Atlantic (TP) and overall or global (ALL).

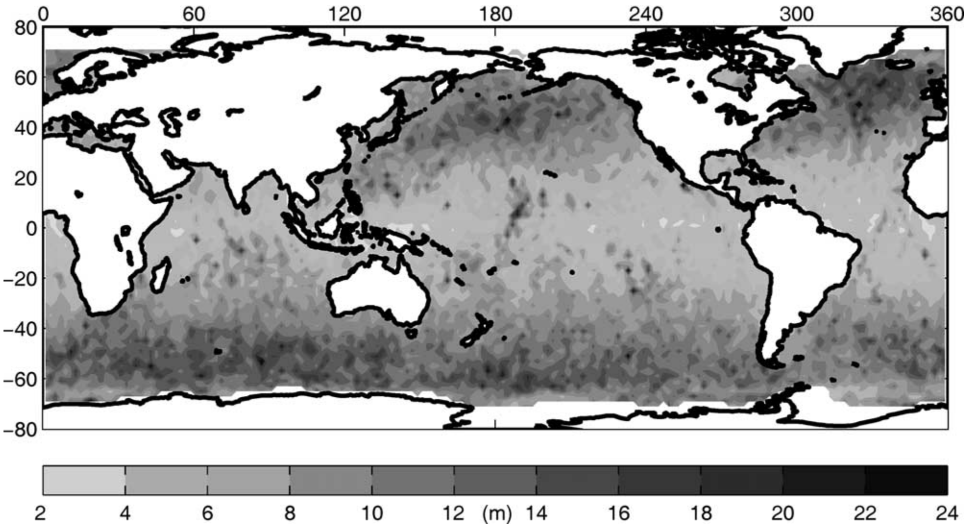

Fig. 12. Global vales of H_s100 computed using POT data from $4° \times 4°$ mesh-elements and the 3PW model.

could be considered homogeneous. On a first approximation, however, these areas could be related to circular regions with diameters consistent with the spatial scale of decorrelation for observations of H_s. Based on the results of Tournadre [5], these would be approximately 200 km for the equator and 60 km at higher latitudes, which lead to regions with sizes of the same order of magnitude of $2° \times 2°$ mesh elements, but much smaller than $4° \times 4°$ areas.

5.2.2. IDM/FT1 approach

Fig. 13 shows the resulting global values of H_s100 computed using IDM data from $2° \times 2°$ mesh-elements and the FT1 model. In contrast to the marked short-scale spatial variability seen in Fig. 10, the global distribution of IDM/FT1 H_s100 is relatively smooth as would be expected from an intuitive perspective. Goodness-of-fit scores associated with the estimates shown in Fig. 13 are shown in Fig. 14. These scores are organized into four categories based on passes or failures at the 95% confidence level of the three statistical tests previously defined (see above).

The percentages of $2° \times 2°$ mesh elements falling into the four score categories for goodness-of-fit (pass three tests, pass any two of three tests, fail any two tests and fail all tests) are summarized in Table 8 within the regions identified in Fig. 9. This table indicates that the IDM data/FT1 model combination provides estimates of H_s100 extrapolated from a statistical model that fails to fit the IDM data in nearly 50% of locations around the globe. Fig. 14 illustrates the global distribution of goodness-of-fit scores associated with the values listed in Table 8.

Despite a generally disappointing performance on a global basis, the IDM/FT1 approach performs very well in terms of goodness-of-fit within the Southern Ocean. The performance is acceptable in most locations in the Tropical Atlantic and Pacific Ocean regions. In northern latitudes of the Pacific and Atlantic the goodness of fit of the IDM/FT1

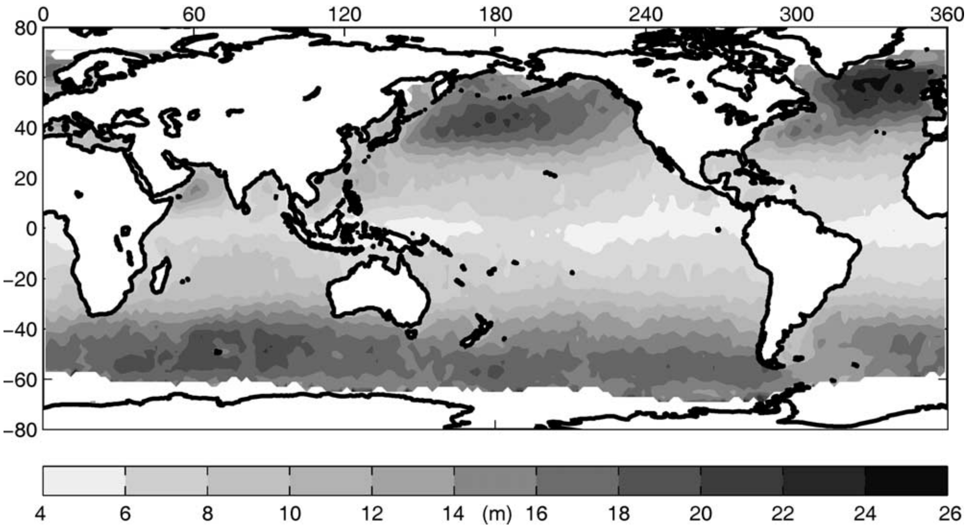

Fig. 13. Global values of H_s100 computed using IDM data from $2° \times 2°$ mesh-elements and the FT1 model.

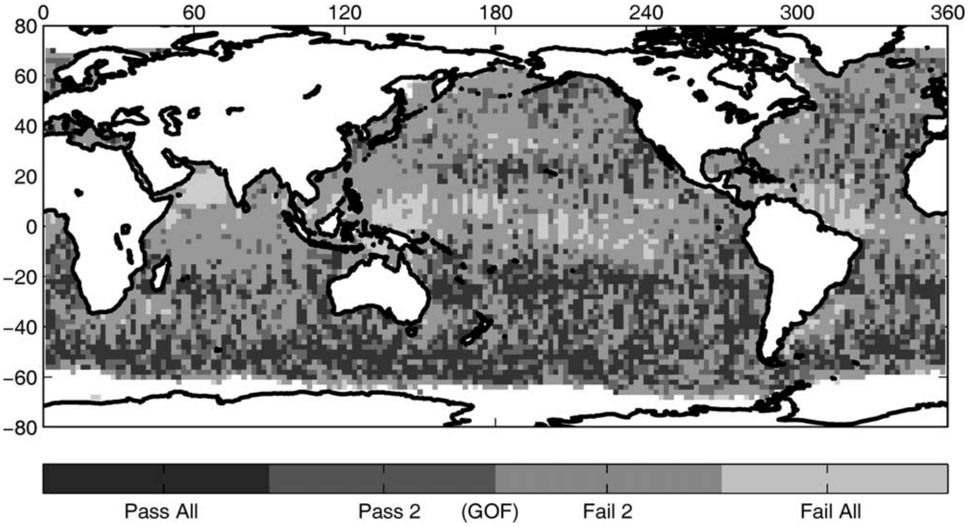

Fig. 14. Goodness of fit scores associated with the values of H_s100 of Fig. 13. The shading levels reflect the number of tests passed/failed at the 95% confidence level.

approach is poor, with locations failing two or three tests in approximately 70% of the cases. The worst goodness-of-fit scores occur in the Indian Ocean, where failure in two or three tests occur in nearly 80% of locations. Within the Indian Ocean region, the Arabian Sea is identified as an area where the IDM/FT1 approach fails all three tests in more than 90% of the locations.

The results of our global analysis once more confirm the validation of satellite-derived H_s100 presented in Section 4, where the goodness-of-fit of long-term extremes passed two or three tests in nearly 50% of the validation sites. We should, however, bear in mind that despite the poor performance in terms of goodness-of-fit, the IDM/FT1 approach provided the satellite-derived estimates of H_s100 best matching the target buoy-derived POT/3PW H_s100 (Section 4). Assuming that these results may be extrapolated to other locations around the globe and considering that the POT/3PW estimates of H_s100 from either $2° \times 2°$ or $4° \times 4°$ generally underestimated the target buoy-derived values, we conclude that the IDM/FT1 approach would be the best choice for determining extreme values of H_s100 computed using satellite altimeter measurements of H_s.

Our validation analysis showed that IDM/FT1 H_s100 computed using data from $2° \times 2°$ or $4° \times 4°$ mesh elements are nearly identical. Again, these outcomes were confirmed by a comparison of global H_s100 at both these resolutions. Although the global distribution of values from $4° \times 4°$ data was slightly smoother than in Fig. 13, the bias was negligible at all locations. Consequently, a global plot of these estimates is not shown.

Goodness-of-fit statistics for H_s100 estimated using the IDM/FT1 approach and $4° \times 4°$ data within the regions identified in Fig. 9 are given in Table 8. Repeating the trend identified for estimates made with the POT/3PW approach, the larger mesh-element size caused a general relative degradation of goodness-of-fit which was even greater than that of the POT/3PW analysis. We believe that this may have resulted from a combination of using data from a region including areas with slightly different wave climatology with the fact that for larger areas the number of IDM points increases accordingly, inducing a decrease of statistical tolerance for differences between the model and empirical CDFs.

Table 8
Percentage of mesh elements satisfying each of the four categories used for assessing goodness-of-fit of IDM data to the FT1 model

Region	$2° \times 2°$				$4° \times 4°$			
	Pass all	Pass 2	Fail 2	Fail all	Pass all	Pass 2	Fail 2	Fail all
SO	37.6	25.0	35.6	1.8	18.0	16.8	58.3	6.9
IO	11.3	13.1	65.7	9.9	4.5	5.7	67.5	22.1
NP	9.3	21.2	65.8	3.6	3.1	6.9	76.2	13.9
TP	20.4	18.5	53.2	7.9	8.3	7.6	63.9	20.2
NA	10.5	24.4	62.6	2.5	3.2	6.5	76.2	14.1
TA	25.5	20.8	46.5	6.6	10.0	12.7	60.3	17.0
ALL	22.9	20.5	50.9	5.7	9.8	15.8	68.5	5.9

Results for $2° \times 2°$ and $4° \times 4°$ mesh elements are indicated. Regions are defined according to Fig. 9 and named as follows: Southern Ocean (SO), Indian Ocean (IO), Northern Pacific (NP), Tropical Pacific (TP), Northern Atlantic (NA), Tropical Atlantic (TP) and overall or global (ALL).

5.2.3. Climatic properties of Extreme H_s

Despite differences between global H_s100 fields shown in Figs. 12 and 13, these figures also show some features that are robust enough to allow a qualitative description of a global climatology of extremes. Consistent with other descriptions of the general properties of the global wave climate [1,3,4,30], among others), the first and most striking feature is the zonal (latitudinal) variation of maxima. Three 'belts' are clearly identified in both hemispheres, as follows:

- A higher latitude region above 40° of latitude toward the poles, where values of H_s100 are typically large;
- An equatorial belt located approximately within the region extending from 20°S to 20°N, dominated by low H_s100; and
- A subtropical or mid-latitude transitional zone between 20 and 40°.

The largest values of computed H_s100, ranging from approximately 15 to 25 m, occur in the high latitude zone, where intense winds develop in association with mid-latitude storm systems or long westerly fetches. Except in areas exposed to hurricanes, the equatorial zone is dominated by persistent trade winds that are, however, not intense enough to generate severe sea states. Consequently, swell generated in higher latitudes are the predominant wave systems within the equatorial belt, which results in H_s100 ranging typically from approximately 5 to 10 m. Subtropical regions form a transitional belt dominated by large atmospheric gyres surrounding semi-permanent high atmospheric pressure areas. Severe sea-states in these regions are usually associated with the propagation of cold fronts and/or the penetration of storms formed in higher latitudes. Values of H_s100 range typically from 8 to 14 m.

However well defined, these zonal belts do not allow the highlighting of some well-marked regional characteristics that are evident after a closer examination of Figs. 12 and 13. A more satisfactory approach is provided by Young [4], who describes regional variations of wind and wave climate over the global ocean within seven climatic zones: northern latitudes, northern sub-tropics, equatorial regions, southern sub-tropics, southern latitudes, Eastern Pacific and Arabian Sea. Excluding the Eastern Pacific region, the remaining zones are also useful for characterizing the distribution of H_s100 on a synoptic scale.

Within the northern latitude region, both North Atlantic and North Pacific basins present similar extreme H_s conditions registering the highest H_s100 on the globe. However, larger areas with H_s100 in excess of 20 m occur within the North Atlantic basin, particularly near the North Sea, suggesting this region is the roughest on the globe. Comparable in roughness to the North Atlantic basin are the southern latitudes, where high H_s100 values are found in the Indian-Southern basin within the 'triple-A triangle' formed by Africa, Australia and Antarctica.

Young [4] considered global mean monthly conditions and argued that sea-states found in the sub-tropical regions, particularly within the Indian, the Pacific and the South Atlantic Oceans, are largely associated with the penetration of swell generated by severe storms in the Southern Ocean and at higher northern latitudes. A milder wave climate in the relatively narrow North Atlantic basin may result from the distribution of land masses that blocks the penetration of swell from higher latitudes.

The extreme conditions represented by the values of H_s100 in the present analysis are more likely associated with local storms, rather than remotely generated swell. The mean monthly global distributions of Young [4] showed 'tongues' of wave height extending from the high latitude storm regions into the sub-tropics and tropics. These features are not evident in the H_s100 fields of Fig. 13. Mean monthly statistics also reveal a more globally uniform wave field than does H_s100. The results of Young [4] showed that, typically, minimum and maximum mean monthly H_s ranged between 1.5 and 5.5 m, a variation of a factor of approximately 3.7. In contrast, H_s100 values vary between 5 and 25 m, a factor of 5.0. Again, these results support the conclusion that mean global values of H_s are largely determined by high latitude storms and the resulting swell propagation, whereas extreme values are largely determined by local storm events.

It should be remembered that the, already highlighted, deficiencies in sampling density of the satellites will have a significant impact on tropical and sub-tropical regions, where tropical cyclones are a dominant forcing event. In these regions, values of H_s100 are likely to be underestimated.

Values of H_s100 seem unusually high within the Arabian Sea, as seen clearly in both Figs. 12 and 13. This region owes its distinctive climatic characteristics to the Asian monsoon. According to Young [4], during the summer monsoon a strong south-westerly jet develops close to the African coast with monthly-mean surface winds exceeding 15 ms^{-1}, which generate severe sea-states associated with values of H_s100 exceeding 14 m.

6. Discussion

The study of Cooper and Forristall [9] concluded that: (A) combining satellite measurements over a radius between 100 and 300 km around the site of interest yields equivalent information to hourly (buoy) measurements at that site, and (B) 100-year (extreme) wave heights can be estimated from satellite data using exactly the same CDF techniques that are used for (buoy) measurements at a site.

Considering the aim of determining long-term extreme values of H_s, the present results, which consider not synthetic but actual satellite and buoy measurements, indicate that statement 'A' may be true or false depending on the chosen approach. In the case of the IDM/FT1 combination, which is very similar to the approach for estimating extremes followed by Cooper and Forristall [9], then this result is valid. However, when the POT/3PW approach is considered it is no longer applicable. In other words, our results indicate that although the satellite may sample H_s from a similar number of storms detected by an in situ device, as indicated by Cooper and Forristall [9] and also by our results when using the IDM/FT1 approach, the satellite database seems to have missed either a larger number of more severe sea states or their periods of stronger intensity, which are ultimately associated with the generation of extremes. This might have led to systematically underestimated satellite-derived H_s100 relative to buoy-derived values.

Our results also show that statement 'B' is applicable exclusively to the IDM/FT1 approach and, in this sense, the results of Cooper and Forristall [9] are totally supported by our analysis. However, they refrain from using POT data claiming that 'it is not yet clear how to apply it to satellite data', since this method depends on knowing a priori the number of storms per year at a given point of interest. In using a deterministic approach to determine yearly storm rates at given oceanic sites, our study extends the analysis of Cooper and Forristall [9] by indicating that undersampling of storm peaks makes approaches using satellite-derived POT data invalid for the purposes of estimating long-term extreme H_s.

The results presented above support the idea that unless the number of satellites orbiting the earth and carrying wave measuring devices is greatly increased, the best approach for computing long-term extremes from satellite data is to evaluate the accuracy and statistical reliability of methods using IDM data. A next step in that direction, which was not pursued in this study, would be to use statistical models other than the FT1 distribution with IDM data.

The conceptual framework justifying the use of IDM data and seeking more reliable statistical distributions fitting the entire observational database may also be extended to the determination of extreme H_s using wind-wave model data. Recent studies of the skill of commonly used operational wind-wave models [2,23,24,31,32] have revealed excellent performance of model outcomes in reproducing near-average sea-state conditions, but significantly poor performance in simulating storm peak H_s in severe forcing conditions. In this sense, H_s data from wind-wave model hindcasts have similar general properties to satellite altimeter measurements. Thus, we may expect that using IDM data to estimate long-term extreme H_s would be a potentially useful path to be followed.

There are many other relevant contributions to the field of investigation concerning the determination of long-term extreme H_s. One important issue that warrants further discussion in the light of the results presented above refers to the time-length in consecutive years needed for producing a statistically-sound time series of H_s. Results of Panchang et al. [21] indicate that values estimated from time series 5 or 14 years long are nearly identical. This result is also supported by our validation analysis presented in Section 4, where nearly identical values of H_s100 were computed from buoy data truncated at the combined satellite database measurement period (nearly 10 years) and the full-length of in situ data (generally over 20 years).

An extensive analysis of this topic is presented in Labeyrie [33], who shows that parameters from models used in extreme analysis vary by much less than 10% when determined from 10- or 100-year-long in situ data sets. He suggests that 'the uncertainty due to the extrapolation step becomes quite negligible; the main difficulty is to establish the limiting law properly'. We conclude this discussion by stressing that our results strongly-support this statement, as these results indicate, in agreement with the final conclusions of Labeyrie [33], that non-standard statistical procedures should be developed for assessing practical approaches for computing long-term extreme wave heights and the associated statistical reliability, given the present limitation inherent to satellite altimeter data.

7. Concluding remarks

The present analysis has considered a 10-year combined database of satellite altimeter observations of H_s. This analysis has shown that such data can be used to obtain reasonable estimates of extreme wave conditions, such as H_s100.

The following conclusions can be drawn:

1. With only a single satellite operational at any one time, the sampling density is such, that not all extreme events will be sampled. Therefore, methods such as POT, which require accurate observations of extremes, will result in an underestimation of H_s100;
2. Methods which use all observed data to estimate extremes, such as IDM, will yield more reliable results in cases where H_s has been underestimated;
3. If IDM is to be used, it is essential that a statistical extrapolation CDF can be fitted to the IDM data and still yield results applicable to extremes. That is, the CDF must not only fit the body of the probability data accurately, but also, critically, the extreme tail;
4. Comparisons with buoy data indicate that IDM data extrapolated using the Fisher-Tippet type I distribution yields acceptable results. There is, however, scope to investigate more appropriate distributions;
5. In order to use satellite data for the prediction of extremes, it is necessary to bin all data from satellite passes through a region around the point of interest. The present results indicate that a square of size $2° \times 2°$ gives acceptable results for this purpose. Larger $4° \times 4°$ squares seem to be so large that they may include data from regions of different climatology;
6. Consistent with previous studies, our results indicate that a satellite database of 10 years duration seems

sufficiently long to obtain consistent extreme value estimates, given the appropriate methodology is chosen.

7. The conceptual framework for estimating extreme H_s from altimeter observations using the FT1 model, in association with IDM data, may also be useful for estimating extremes from wave model data.

Acknowledgements

This study is part of research activities sponsored by the Conselho Nacional de Desenvolvimento Cientifico e Tecnologico (CNPq), Brazil. Both authors greatfully acknowledge the support granted by the School of Mathematics (UNSW), the School of Civil Engineering (ADFA/UNSW) and the Faculty of Engineering, Computer and Mathematical Sciences, the University of Adelaide during several stages of development of the study.

References

[1] Barstow SF. World wave atlas. AVISO Altimetry Newsletter 1996;4: 24–5.
[2] Cardone VJ, Jensen RE, Resio DT, Swail VR, Cox AT. Evaluation of contemporary ocean wave models in rare extreme events: the Halloween storm of October and the storm of the century of March 1993. Journal of Atmosphere and Ocean Technology 1996;13: 198–230.
[3] Carter DJT. Estimating extreme wave heights in the NE Atlantic from GEOSAT data. Offshore Tech. Report, OTH93-396. London (UK): Health and Safety Executive; 1993.
[4] Young IR. Seasonal variability of the global ocean wind and wave climate. International Journal of Climatology 1999;19:931–50.
[5] Tournadre J. Time and space scales of significant wave heights. Journal of Geophysical Research 1993;69B:4727–38.
[6] Carter DJT, Challenor PG. Metocean parameters—wave parameters. Part 2: estimation of extreme waves. UK Department of Energy, OTH89-300, London: HMSO; 1990.
[7] Cheney RE, Doyle NS, Douglas BC, Agreen RW, Miller L, Timmerman EL, McAdoo DC. The complete GEOSAT Altimeter GDR Handbook. NOAA Manual NOS NGS 7; 1991. 77 p.
[8] Conover WJ. Practical non-parametric statistics. New York: Wiley; 1980. 493 p.
[9] Cooper CK, Forristall GZ. The use of satellite altimeter data to estimate extreme wave climate. Journal of Atmospheric and Oceanic Technology 1997;14(2):254–66.
[10] Daniels RC, Birdwell KR. A storm climatology data base with applications in regional and global change studies. Bulletin of American Meteorological Society 1991;72(7):1005–7.
[11] ESA, ERS-1 User Handbook. European Space Agency. ESA SP-1148, ESTEC Publishing Division; 1993. 129 p.
[12] Fu L-L, Christensen EJ, Yamarone CA, Lefebvre M, Menard Y, Dorrer M, Escudier P. TOPEX/POSEIDON mission overview. Journal of Geophysical Research 1994;99:24369–81.
[13] Goda Y. On the methodology of selecting design wave height. Proceedings of the 21st International Conference on Coastal Engineering, Malaga, Spain; 1988. p. 899–913.
[14] Goda Y, Kobune K. Distribution function fitting for storm wave data. Proceedings of the 22nd International Conference on Coastal Engineering, Delft, Netherlands; 1990. p. 899–913.
[15] Goda Y, Hawkes P, Mansard E, Martin MJ, Mathiesen M, Peltier E, Thompson E, van Vledder G. Intercomparison of extremal wave analysis methods using numerically simulated data. Proceedings of 2nd Symposium on Ocean Wave Measurement and Analysis, New Orleans, USA; 1993. p. 963–977.
[16] Greenslade DJM, Young IR. The effect of altimeter sampling patterns on estimates of wave model error correlations. 7th International Workshop on Wave Hindcasting and Forecasting, Banff, Alberta, Meteorological Service of Canada; 2002. p. 445–457.
[17] Guedes-Soares C, Lopes LC, Costa MDS. Wave climate modelling for engineering purposes. In: Schreffler BA, Zienkiewicz OC, editors. Computer modelling in ocean engineering. Balkema; 1988. p. 169–75.
[18] Kalnay E, Kanamitsu M, Kistler R, Collins W, Deaven D, Handin L, Iredell M, Saha S, White G, Woollen J, Zhu Y, Chelliah M, Ebisuzaki W, Higgins W, Janowiak J, Mo KC, Ropelewski C, Wang J, Leetmaa A, Renolds R, Jenne R. The NCEP/NCAR 40-year re-analysis Project. Bulletin of American Meteorology 1996;77:437–71.
[19] Mathiesen M, Goda Y, Hawkes P, Mansard E, Martin MJ, Peltier E, Thompson E, van Vledder G. Recommended practice for extreme wave analysis. Journal of Hydraulic Research 1994;32(6):803–14.
[20] Muir LR, El-Shaarawi AH. On the calculation of extreme wave heights: a review. Ocean Engineering 1986;13(1):93–118.
[21] Panchang V, Zhao L, Demirbilek Z. Estimation of extreme wave heights using Geosat measurements. Ocean Engineering 1998;26: 205–25.
[22] Snedecor GW, Cochran WG. Statistical methods, 8th ed. Ames, IA: Iowa State University; 1989.
[23] Sterl A, Komen GJ, Cotton PD. Fifteen years of global wave hindcasts using winds from the European Centre for Medium-Range Weather Forecasts reanalysis. Journal of Geophysical Research 1998;C103: 5477–92.
[24] Swail VR, Cox AT. On the use of NCEP-NCAR reanalysis surface marine wind fields for a long-term North Atlantic wave hindcast. Journal of Atmospheric Ocean Technology 2000;17(4):532–45.
[25] Teng CC. Long-term and extreme waves in the Gulf of Mexico. Proceedings of Conference on Ocean Wave Kinematics, Dynamics and Loads on Structures, Houston, Texas; 1998. p. 342–349.
[26] Tournadre J, Ezraty R. Local climatology of wind and sea state by means of satellite radar altimeter measurements. Journal of Geophysical Research 1990;95(C10):18255–68.
[27] Tucker MJ. Waves in ocean engineering: measurement, analysis, interpretation. Ellis Horwood Series in Marine Sciences, London: Ellis Horwood; 1991. 431 p.
[28] Van Vledder G, Goda Y, Hawkes P, Mansard E, Martin MJ, Mathiesen M, Peltier E. Case studies of extreme wave analysis. Proceedings of 2nd Symposium on Ocean Wave Measurement and Analysis, New Orleans, USA; 1993. p. 978–992.
[29] Young IR. An intercomparison of GEOSAT, TOPEX and ERS1 measurements of wind speed and wave height. Ocean Engineering 1998;26:67–81.
[30] Young IR, Holland GJ. Atlas of the oceans: wind and wave climate. New York: Pergamon Press; 1996. 241 p.
[31] Wang XLL, Swail VR. Changes of extreme wave heights in Northern Hemisphere oceans and related atmospheric circulation regimes. Journal of Climate 2001;14(10):2204–21.
[32] Wang XLL, Swail VR. Trends of Atlantic wave extremes as simulated in a 40-yr wave hindcast using kinematically reanalyzed wind fields. Journal of Climate 2002;15(9):1020–35.
[33] Labeyrie J. Timescales and statistical uncertainties in the prediction of extreme environmental conditions. Reliability Engineering and Safety Systems 1991;32:243–66.